Copyright

by

Rohit Bezewada

2013

The Thesis Committee for Rohit Bezewada
Certifies that this is the approved version of the following thesis:

Effect of Crystal Size on Diffraction Contrast of a Screw Dislocation

APPROVED BY
SUPERVISING COMMITTEE:

Supervisor:

____
Paulo Ferreira

____
Gregory J. Rodin

Effect of Crystal Size on Diffraction Contrast of a Screw Dislocation

by

Rohit Bezewada,B.Tech

Thesis

Presented to the Faculty of the Graduate School of

The University of Texas at Austin

in Partial Fulfillment

of the Requirements

for the Degree of

Master of Science in Engineering

The University of Texas at Austin

August 2013

Acknowledgements

First and foremost I would like to thank my advisor Professor Paulo Ferreira for guidance and constant encouragement throughout my graduate school experience. I express my gratitude to all the trust he placed in my abilities, and giving me so many opportunities to make the most out of graduate school. I learn leadership skills seeing the way he led the research group, he was always approachable and was one of the most compassionate people I have met. Working with him truly has been a life changing learning experience.

I would also like to thank Professor Greg Rodin for his time and effort in providing me valuable guidance and suggestions through the course of my work. I am greatly indebted to him as he was instrumental in shaping my understanding of my research. I would like to thank him for patiently answering my numerous questions pertaining to my computations.

I would like to thank Virgilio for his invaluable inputs and extensive help with all the programming. I would like to thank my colleagues Rosa Calinas, Charles Amos, Somaye Rasouli, Karalee Jarvis and Kang Yu for their support and discussions during the course of my graduate studies.

I would love to thank my roommate and friend Jean-Gil Gutierrez for being with me at every little step. I would like to thank my girlfriend Danica Brown who believed in me, encouraged me all along and made me realize a lot of what I was capable of achieving. I cannot thank you enough mom and dad for your love, patience, unflinching faith and unwavering support.

Abstract

Effect of Crystal Size on Diffraction Contrast of a Screw Dislocation

Rohit Bezewada, MSE

The University of Texas at Austin, 2013

Supervisor: Paulo Ferreira

As materials get reduced in size down to the nanoscale it becomes more complex to characterize them. In this regard transmission electron microscopy has been extensively used to better characterize and understand the mechanical behavior of materials at the nanoscale, although there are various contrast mechanisms that can be used in a TEM micrograph. Focusing in particular on diffraction contrast, we know that dislocation lines are interpreted based on how the displacement field of a dislocation in an infinite crystal influences contrast. However, from a practical standpoint most of the samples that are used in microscopy are of a finite size. Thus, it is important to understand the change in contrast of a screw dislocation by taking into account the effect of crystal size. A MATLAB program has been written to simulate contrast in the TEM of a screw dislocation, taking into account the modified displacement fields for finite size crystals. The effect of reducing crystal size and the effect of microscopic parameters, such as the deviation parameter and g.b diffraction conditions have been also analyzed.

Table of Contents

List of Figures

Chapter 1: Introduction

1.1 Motivation

Nanoparticles play an increasingly important role in a wide variety of fields including drug delivery, materials for medicine, next generation display materials, hydrogen storage materials, to name a few. These applications can be greatly improved by better understanding the properties at the nanoscale. Among these properties, the mechanical behavior of nanoparticles is of great interest for various applications.

An earlier experiment showed that defect-free single crystalline silicon particles with radii ranging from 20 to 50 nm demonstrated hardness values up to 50 GPa, which is four times greater than that of bulk silicon. This was explained by the high level of plastic strain and work hardening experienced by very small volumes. The plastic deformation was claimed to be due to heterogeneous dislocation nucleation at the contact edges [1]. This theory however was challenged based on the fact that dislocation activity is either prohibited or unstable due to image forces that tend to push dislocations out of the nanoparticle. The above experiment clearly demonstrates that it is critical to be able to characterize materials at the nanoscale in order to understand the effect of defects, in particular dislocations, on the mechanical behavior of materials.

However, the characterization of dislocations using transmission electron microscopy can get quite complex. There are various contrast mechanisms to interpret in a TEM micrograph. Diffraction contrast is widely used to interpret dislocation images. Yet, when considering the presence of a dislocation in a nanoparticle, the displacement field around a dislocation may be affected by the existence of the nearby surfaces, which could influence contrast.Thus, this thesis focuses on determining the effect of crystal size on the dislocation displacement field and consequently on the diffraction contrast observed in a TEM image.

The concept of a dislocation has been proposed since the 20^{th} century [2]. Later work has predicted the existence of lattice imperfections and explained slip in grains due to plastic deformation [3-5].The role dislocation plays in elasto-plastic deformation has been analyzed by many researchers [6-11]. Analysis of dislocation problems in inhomogeneous media, which help better understand the behaviour of dislocations near interface boundaries have been extensively analyzed [12-14]. Situations where the image forces become significant occur when a dislocation is close to a surface or when the dislocations are in a nanocrystal. The case of when a dislocation is near an interface can be analyzed in semi-infinite crystals [15]. Forces experienced by a dislocation near a surface film are calculated by using an infinite set of image dislocations [16]. However, in the case of nanocrystals, more than one surface may be close to the dislocation and the net force experienced by the dislocation would be a superposition of all the image forces. Additionally, with decreasing size, the stress field analysis more complex. Finite element method and boundary element methods have been used to solve this elastic boundary problem. There has extensive stress field analysis for dislocations in nanocrystals and continuous media [17-20]. These stress fields are numerical solutions and are complex. Despite this work, the elastic field solutions obtained so far cannot be used as input displacement fields for solving the Howie-Whelan equations. In order to address this issue and to determine the effect of reducing crystal size on the diffraction contrast in a TEM this thesis provides the solutions for a screw dislocation surrounded by traction free surfaces.

1.2 The Approach

To perform the intensity contrast simulations for the presence of dislocations in a finite crystal, the first step is to obtain a solution for the Howie Whelan Equations. This is achieved by writing a Matlab code that takes into account the dynamical interaction of electrons with the sample. The diffraction conditions, material properties and the sample parameters are all encoded in the program. Under these conditions, the code is able to obtain the bright and dark field contrast profiles of a dislocation in a finite crystal. In order to see how a finite crystal effects the displacement field of a dislocation , the case of a screw dislocation was taken, as its elastic field in not as complex as for edge or mixed dislocations.

Subsequently, three cases are investigated, namely 1) infinite crystal, 2) semi-infinite crystal and 3) finite crystal. In the end, the simulations show how the image of a dislocation varies with the finite size of the crystal. The effect of microscopic parameters on the contrast profiles, with changing crystal size is also analyzed.

1.3 THESIS AND ITS MAIN CONTRIBUTIONS

The main contributions of the thesis are:

1. Development of a Matlab program that solves the Howie Whelan Equations for a two beam case. The program gives us the direct and diffracted beam intensity values, which are used to obtain intensity contrast profiles for the case of a single screw dislocation.
2. Solving the elastic field for the case of an semi-infinite crystal and creating a subroutine in the program to run the simulations for this particular case.
3. Solving the elastic field for the case of a finite crystal, when there are two surfaces around the dislocation. This is done by solving for the case of a periodic array of dislocations.
4. Analyzing the intensity contrast profiles for the various cases to study the effect of crystal size on dislocation contrast.
5. Analyzing the effect of microscopic parameters on dislocation contrast with changes in crystal size.

1.4 OUTLINE OF SUBSEQUENT CHAPTERS

Chapter 2 starts by discussing the Howie- Whelan equations. It explains the mathematics behind how the intensity contrast is obtained. It first introduces the Howie-Whelan equations for the case of a perfect crystal. This is followed by explaining how the equations are modified if there is a defect present in the crystal. The idea behind this chapter is to introduce the contribution of the displacement field of a defect when trying to obtain the solutions for the

Howie-Whelan Equations. The contrast profiles that are seen consider the displacement field of a dislocation to be for an infinite crystal.

Chapter 3 talks about the displacement field for an infinite crystal. The solutions obtained for the elastic fields for a semi-infinite crystal and a crystal with the two vertical traction free surfaces are discussed in detail. This discussion helps understand the input displacement fields to the simulation program.

Chapter 4 shows the results of all the simulations and discusses the effect of the reducing crystal size on the dislocation contrast width. The effects of the microscopic parameters such as deviation conditions and g.b conditions are discussed. The discussion helps throw light on how contrast is influenced when reducing the size of the crystal.

Chapter 2: Howie Whelan Equations

2.1 INTRODUCTION

When imaging using diffraction contrast in the TEM, the varying intensity of the diffracted beams in different regions of the sample is the quantity of interest. These intensity variations occur due to changes in diffracting conditions. As a result, the contrast features we observe in a TEM micrograph, when diffraction contrast is used, is determined by calculating the intensity of the electron beam or beams across the different regions in the image. However, the calculation of intensities in the TEM is not trivial. Consider an electron beam incident on a crystal which is oriented close to the Bragg diffracting condition for a particular set of planes. As the beam transverses through the crystal it will generate a diffracted beam which, in turn, can be re-diffracted back into the incident direction. This dynamic exchange of electrons between the incident and diffracted beams may occur several times if the crystal is thick. This dynamical behaviour has to be accounted for, while calculating the intensities, unless the sample is very thin.

Fortunately, dynamical diffraction can be mathematically modeled by the so-called Howie Whelan equations, where the scattering of electrons from the main beam into the diffracted beam and the subsequent scattering from the diffracted beam back into the main beam is taken into account. In addition, two are assumptions are considered for the model, namely 1) the two beam approximation where the intensity is related with the interaction of only two beams; the transmitted beam and a diffracted beam, and 2) the column approximation, which considers the crystal divided into parallel independent columns, with dynamic exchange between incident and diffracted beams within a column, but no exchange of electrons between columns.

Next, I will discuss in greater detail the basis for the Howie-Whelan equation for the cases of a perfect crystal and a crystal with defects.

2.2 THE HOWIE WHELAN EQUATIONS FOR A PERFECT CRYSTAL

The two beam dynamical theory can be formulated in two ways: The first way is the wave optical formulation in which electrons are considered to be waves and are assumed to be diffracted by the crystal in much the same way as monochromatic light is diffracted by grating. In the second approach a wave mechanical formulation is considered where the electrons are particles moving in the potential field of the crystal and the Schrodinger equation for this situation is set up and solved. Both these approaches lead to the same pair of coupled differential equations. The derivation of these equations is beyond the scope of this thesis and can be found elsewhere [20-22]. The coupled differential equations can be expressed as:

$$\frac{d\phi_g}{dy} = \frac{\pi i}{\xi_g}\phi_0 e^{-2\pi i(g+s)r} + \frac{\pi i}{\xi_0}\phi_g \tag{2.1}$$

$$\frac{d\phi_0}{dy} = \frac{\pi i}{\xi_g}\phi_g e^{2\pi i(g+s)\mathrm{r}} + \frac{\pi i}{\xi_0}\phi_0 \tag{2.2}$$

where ϕ_g denotes the amplitude of the diffracted beam, ϕ_0 denotes the amplitude of the direct beam, ξ_0 is the characteristic length for forward scattering, i.e. scattering from any beam into itself, ξ_g is called the extinction distance which is a measure of periodic distance in the crystal over which the diffracted beam builds up and fades away, s is the parameter that measures the deviation of the crystal orientation from the exact Bragg position, r is the lattice vector, y is the direction of the incident beam (in the case of column approximation it is the coordinate along the column) and g is the diffracting vector.

In order to simplify eqs. (2.1) and (2.2), an assumption is made that s and r are parallel to y. Under these conditions we get:

$$e^{-2\pi is.r} = e^{-2\pi is.y} \tag{2.3}$$

Using the simplification in eq. (2.3), we can modify eqs. (2.1) and (2.2) to get:

$$\frac{d\phi_g}{dy} = \frac{\pi i}{\xi_g}\phi_0 e^{-2\pi isy} + \frac{\pi i}{\xi_0}\phi_g \qquad (2.4)$$

$$\frac{d\phi_0}{dy} = \frac{\pi i}{\xi_g}\phi_g e^{2\pi isy} + \frac{\pi i}{\xi_0}\phi_0 \qquad (2.5)$$

The coupled differential eqs in (2.4) and (2.5) are known as the Howie-Whelan equations. They reveal that the change in ϕ_g depends on the magnitudes of both ϕ_g and ϕ_0 .Thus, ϕ_g and ϕ_0 are dynamically coupled. These equations can be used to obtain the amplitudes and thereby the intensities ($I \propto |\phi|^2$) for the direct and diffracted beams for a perfect crystal.

2.3 The Modified Howie-Whelan Equations for Crystals with Defects.

The Howie-Whelan equations (2.4) and (2.5) can be modified to include a lattice distortion $R(r)$. A unit cell in a strained crystal will be displaced from its perfect crystal so that it is located at position r' instead of r , given by

$$r' = r + R(r) \qquad (2.6)$$

where $R(r)$ signifies that the lattice distortion can vary throughout the specimen. The term $e^{2\pi i(g+s)r}$ in equation (1) now becomes $e^{2\pi i(g+s)r'}$, which introduces the term $(\mathrm{g}+\mathrm{s}).r'$, given by

$$(\mathrm{g}+\mathrm{s}).r' = (g+s).(r+R) = g.r + g.R + s.r + s.R \qquad (2.7)$$

As r is a lattice vector, $g.r$ becomes an integer. The term $s.r$ can be approximated to $s.z$ since the diffraction planes are parallel to the beam (along z). Also as the deviation parameter s is small and R is small on the basis of elasticity theory, $s.R$ can be ignored. As a result, the modified Howie-Whelan Equations related to a distorted crystal can be written as

$$\frac{d\phi_g}{dy} = \frac{\pi i}{\xi_g}\phi_0 e^{(-2\pi isy - 2\pi ig.R)} + \frac{\pi i}{\xi_0}\phi_g \tag{2.8}$$

$$\frac{d\phi_0}{dy} = \frac{\pi i}{\xi_g}\phi_g e^{(2\pi isy + 2\pi ig.R)} + \frac{\pi i}{\xi_0}\phi_0 \tag{2.9}$$

The new parameter R represents the displacement field at a depth y in the column. In order to obtain results from this theory that are in agreement with experimental observations, the effect of absorption needs also to be taken into account [22-23] Thus, the quantities $\frac{1}{\xi_0}$ and $\frac{1}{\xi_g}$ in equations (2.8) and (2.9) are replaced by the complex quantities $\frac{1}{\xi_0}+\frac{1}{\xi_0'}$ and $\frac{1}{\xi_g}+\frac{1}{\xi_g'}$ respectively. This gives,

$$\frac{d\phi_g}{dy} = \pi i(\frac{1}{\xi_g}+\frac{1}{\xi_g'})\phi_0 e^{(-2\pi isy - 2\pi ig.R)} + \pi i(\frac{1}{\xi_0}+\frac{1}{\xi_0'})\phi_g \tag{2.10}$$

$$\frac{d\phi_0}{dy} = \pi i(\frac{1}{\xi_g}+\frac{1}{\xi_g'})\phi_g e^{(2\pi isy + 2\pi ig.R)} + \pi i(\frac{1}{\xi_0}+\frac{1}{\xi_0'})\phi_0 \tag{2.11}$$

The occurrence of ξ_0' and ξ_g' in equations (2.10) and (2.11) effectively introduces the phenomena of absorption and anomalous absorption into the theory. The quantity ξ_0' determines the mean absorption coefficient of the crystal. The parameter ξ_g' is the two-beam anomalous extinction distance, which takes into account the use of complex crystal potential to justify the anomalous absorption effect.

Equations (2.10) and (2.11) can be further simplified by making a transformation of variables, in the form

$$\phi_0' = \phi_0 e^{(\frac{-\pi iy}{\xi_0})} \tag{2.12}$$

$$\phi_g' = \phi_g e^{(2\pi isy - \pi iy/\xi_0 + 2\pi ig.R)} \tag{2.13}$$

The quantities $\phi_0^{'}$ and $\phi_g^{'}$ are related to ϕ_0 and ϕ_g by phase factors which depend on z. Using the transformations (2.12) and (2.13) and simplifying equation (2.10) and (2.11) we get,

$$\frac{d\phi_0^{'}}{dy} = (-\frac{\pi}{\xi_o^{'}})\phi_0^{'} + \pi i(\frac{1}{\xi_g} + \frac{i}{\xi_g^{'}})\phi_g^{'} \tag{2.14}$$

$$\frac{d\phi_g^{'}}{dy} = \pi i(\frac{1}{\xi_g} + \frac{i}{\xi_g^{'}})\phi_0^{'} + \phi_g^{'}(-\frac{\pi}{\xi_0^{'}} + 2\pi is + 2\pi i\frac{d(g.R)}{dy}) \tag{2.15}$$

When the equations are expressed in the form shown in (2.14) and (2.15), the distortions in the crystal due to the presence of the defect give rise to a local rotation of the lattice and thus the deviation parameter is effectively changed from s to $s + \frac{d(g.R)}{dy}$ (Hirsch et al.,1965,p 164). However s is considered to be a constant down the column approximation, while the term $\frac{d(g.R)}{dy}$ is not because R, the displacement field is continuously varying with y. Therefore, in order to simplify the numerical integration process it is convenient to normalize equations (2.14) and (2.15) so that the expressions are unit-less. This can be done by taking the unit of length to be $\frac{\xi_g}{\pi}$ and changing the variable y in equations (2.14) and (2.15) to Y, where $Y = \frac{y\pi}{\xi_g}$. When this transformation is done in equations (2.14) and (2.15) we obtain,

$$\frac{d\phi_0^{'}}{dY} = (-\frac{\xi_g}{\xi_o^{'}})\phi_0^{'} + (i - \frac{\xi_g}{\xi_g^{'}})\phi_g^{'} \tag{2.16}$$

$$\frac{d\phi_g^{'}}{dY} = (i - \frac{\xi_g}{\xi_g^{'}})\phi_0^{'} + (-\frac{\xi_g}{\xi_0^{'}} + 2is\xi_g + 2\pi i\frac{d(g.R)}{dY})\phi_g^{'} \tag{2.17}$$

When using these equations, the quantity of interest is usually the intensity of the electron waves ($|\phi_0^{'}|^2$ or $|\phi_g^{'}|^2$) rather than the amplitudes , since the intensity is what is recorded on the CCD camera. Thus the phase difference between ϕ_0 and $\phi_0^{'}$ or ϕ_g and $\phi_g^{'}$ can be neglected.

The product $s\xi_g$ is dimensionless and should be denoted by w. The dimensionless ratio $\frac{\xi_g}{\xi_0^{'}}$ is termed as the normal absorption coefficient, and it takes into account the reduction in the number of electrons in the column as a function of depth in the crystal. The ratio $\frac{\xi_g}{\xi_g^{'}}$ is called the anomalous absorption coefficient.

As seen in this chapter, the elastic field associated with the presence of defects in imperfect crystals influences the intensity values that are of interest with regards to diffraction contrast. Thus, in the next chapter we shall investigate the elastic field of dislocations in an infinite crystal and determine how the elastic field for the particular case of a screw dislocation changes with respect to the size of the crystal.

Chapter 3: Elastic field of a screw dislocation as a function of crystal size

3.1 INTRODUCTION

The effect of dislocations on the properties of a crystal is associated with their internal strain and stress field. Therefore, the elastic properties of straight dislocations can be calculated on the basis of linear elasticity theory. Consider first the shear strain given by [24]

$$\varepsilon_{ij} = \frac{1}{2}\left(\frac{du_i}{dx_j} + \frac{du_j}{dx_i}\right) \tag{3.1}$$

where ε_{ij} is the shear strain for when $i \neq j$, u_i is the displacement field component along the i direction, $\frac{du_i}{dx_j}$ is the first derivative of the displacement field component along the i direction with respect to x_j which denotes the j-direction. Now the shear stress can be related to the shear strain by

$$\sigma_{ij} = 2G\varepsilon_{ij} \tag{3.2}$$

where σ_{ij} is the shear stress and G is the shear modulus.

For straight dislocation in an infinite, continuous, isotropic media, the treatment is straightforward for edge, screw and mixed dislocations. However, in a finite body, the displacements and stresses around a dislocation depend on the external surface. Thus, the mathematical treatment is simpler for screw dislocations compared to that for edge dislocations. As result, for the scope of this dissertation, I will consider only screw dislocations.

3.2 NO BOUNDING SURFACES

The case of a single dislocation

Consider the case of a single dislocation in an infinite medium. The screw dislocation line is along the z axis (Fig.3.1) and thus, the displacements along u_x and u_y are zero. The displacement field is given by [24]

$$u_z = \frac{b}{2\pi}\tan^{-1}\frac{y}{x} \qquad (3.3)$$

where *b* is the Burgers vector.

Using relations (3.1) and (3.2) we obtain

$$\sigma_{xz} = \frac{-Gb}{2\pi}\left(\frac{y}{x^2+y^2}\right) \qquad (3.4)$$

$$\sigma_{yz} = \frac{Gb}{2\pi}\left(\frac{x}{x^2+y^2}\right) \qquad (3.5)$$

$$\sigma_{xy} = \sigma_{xx} = \sigma_{yy} = \sigma_{zz} = 0 \qquad (3.6)$$

These relations give us the stress fields for the case of a dislocation in an infinite crystal. However in the case of finite crystal these stress fields would change in the presence of a free surface. This modification is studied first for the case of one bounding surface- the case of a semi-infinite crystal and the corresponding elastic field calculated.

3.3 ONE BOUNDING SURFACE

In a semi-infinite body, a dislocation near a free surface experiences a force, which is called the image force. The force can be calculated assuming a negative hypothetical dislocation on the other side of the surface. In a semi-finite crystal the surface will contribute to an ‘image

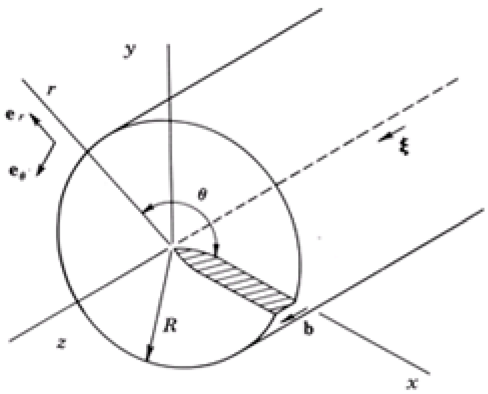

Fig. 3.1: Elastic distortion in a cylinder produced by a screw dislocation along the *z* direction [25].

dislocation' and the total force experienced by the dislocation will be a superposition of these 'image forces' [24].

For the boundary conditions to be met at the free surface we need to add to the stress field of a screw dislocation in an infinite body (equations 3.4 and 3.5), the stress field of an imaginary screw dislocation of opposite sign at *x=-2d* (See figure 3.2).

The stress field of an imaginary screw dislocation of opposite sign in the original coordinate system (origin assumed to be at the core of the screw dislocation) is given by:

$$\sigma_{xz} = \frac{Gb}{2\pi}\left(\frac{y}{((x+2d)^2+y^2)}\right) \tag{3.7}$$

$$\sigma_{yz} = -\frac{Gb}{2\pi}\left(\frac{(x+2d)}{((x+2d)^2+y^2)}\right) \tag{3.8}$$

On adding equations (3.7) and (3.8) to the equations (3.4) and (3.5) we get the modified stress fields for a screw dislocation in the case of one bounding surface which are given by:

$$\sigma_{xz} = -\frac{Gb}{2\pi}\left(\frac{y}{(x^2+y^2)}\right)+\frac{Gb}{2\pi}\left(\frac{y}{((x+2d)^2+y^2)}\right) \tag{3.9}$$

$$\sigma_{yz} = +\frac{Gb}{2\pi}\left(\frac{x}{(x^2+y^2)}\right)-\frac{Gb}{2\pi}\left(\frac{(x+2d)}{((x+2d)^2+y^2)}\right) \tag{3.10}$$

These are the modified stress fields for the case of the semi-infinite crystal. Now if we add an additional surface to try and calculate the modified elastic field, we have to try and obtain traction free surfaces. The calculations used to obtain stress fields for the cases of two vertical and two horizontal surfaces have been shown in the following section.

3.4 TWO BOUNDING SURFACES

3.4.1 The case of Vertical Surfaces

In order to obtain traction free vertical surfaces around a screw dislocation, we start by considering a dislocation near one bounding surface and assume an image dislocation to satisfy the boundary conditions at the free surface as discussed in section 3.3. However, if an additional surface and corresponding image dislocation is placed on the other side of the screw dislocation, the resulting vertical surfaces are not traction free. To address this issue, an infinite periodic array of dislocations of alternating nature (positive and negative screw dislocations) must be considered along the x-axis in order to obtain traction free conditions at those two surfaces. The periodic array is shown in Figure 3.3.

To obtain the stress field due to the periodic array of dislocations we sum the stress fields due to the individual dislocations, given by

$$\sigma_{yz} = \frac{\mu b}{2\pi}\left(\sum_{-\infty}^{\infty}\frac{(x-4nd)}{(x-4nd)^2+y^2} - \sum_{-\infty}^{\infty}\frac{(x+2d-4nd)}{(x+2d-4nd)^2+y^2}\right) \tag{3.11}$$

$$\sigma_{xz} = \frac{-\mu b}{2\pi}\left(\sum_{-\infty}^{\infty}\frac{y}{(x-4nd)^2+y^2} - \sum_{-\infty}^{\infty}\frac{y}{(x+2d-4nd)^2+y^2}\right) \tag{3.12}$$

where μ denotes the shear modulus, b the magnitude of the Burgers vector, and d is the distance between the surface and the core of the dislocation.

Hirth and Lothe (1982) provided some assumptions to use to help simplify the summation to obtain the solution for a periodic array of screw dislocations [25] which gives:

$$\sum_{-\infty}^{\infty}\frac{(\mathrm{n}+p)}{(n+p)^2+q^2}=\frac{\pi\sin(2\pi p)}{\cosh(2\pi q)-\cos(2\pi p)} \tag{3.13}$$

$$\sum_{-\infty}^{\infty}\frac{1}{(n+p)^2+q^2}=\frac{\pi\sinh(2\pi q)}{\mathrm{q}(\cosh(2\pi q)-\cos(2\pi p))} \tag{3.14}$$

Comparing equations (3.11) and (3.12) to equations (3.13) and (3.14) we can rewrite equations (3.11) and (3.12) as:

$$\sigma_{yz}=\frac{\mu b}{8d}\left(\frac{\sin(\frac{\pi x}{2d})}{\cosh(\frac{\pi y}{2d})-\cos(\frac{\pi x}{2d})}-\frac{\sin(\frac{\pi(x+2d)}{2d})}{\cosh(\frac{\pi y}{2d})-\cos(\frac{\pi(x+2d)}{2d})}\right) \tag{3.15}$$

$$\sigma_{xz}=\frac{-\mu b}{8d}\left(\frac{\sinh(\frac{\pi y}{2d})}{\cosh(\frac{\pi y}{2d})-\cos(\frac{\pi x}{2d})}-\frac{\sinh(\frac{\pi y}{2d})}{\cosh(\frac{\pi y}{2d})-\cos(\frac{\pi(x+2d)}{2d})}\right) \tag{3.16}$$

As shown in equation (3.16), $\sigma_{xz}=0$ for $x=\pm d$. Thus, we satisfy the boundary conditions for the two vertical surfaces and have the elastic fields due to the periodic array of dislocations along the x-axis.

3.4.2 The case of Horizontal Surfaces

In order to obtain traction free horizontal surfaces we assume an infinite periodic array of dislocations along the y-axis of alternating nature (positive and negative screw dislocations). The periodic array is shown in Figure 3.4. To obtain the stress field due to the periodic array of dislocations we have to sum the stress fields due to the individual dislocations:

$$\sigma_{yz}=\frac{\mu b}{2\pi}\left(\sum_{-\infty}^{\infty}\frac{x}{x^2+(y-4nd)^2}-\sum_{-\infty}^{\infty}\frac{x}{x^2+(y-4nd)^2}\right) \tag{3.17}$$

$$\sigma_{xz} = \frac{-\mu b}{2\pi}\left(\sum_{-\infty}^{\infty}\frac{(y-4nd)}{x^2+(y-4nd)^2} - \sum_{-\infty}^{\infty}\frac{(y-4nd)}{x^2+(y-4nd)^2}\right) \tag{3.18}$$

where μ denotes the shear modulus, b the magnitude of the Burgers vector, and d is the distance between the surface and the core of the dislocation. In order to obtain traction free horizontal surfaces we should have $\sigma_{yz} = 0$, for $y = \pm d$.

Comparing equations (3.17) and (3.14) we can rewrite equation (3.17) as

$$\sigma_{yz} = \frac{-\mu b}{8d}\left(\frac{\sinh(\frac{\pi x}{2d})}{\cosh(\frac{\pi x}{2d}) - \cos(\frac{\pi y}{2d})} - \frac{\sinh(\frac{\pi x}{2d})}{\cosh(\frac{\pi x}{2d}) - \cos(\frac{\pi(\mathrm{y}+2d)}{2d})}\right) \tag{3.19}$$

As shown in equation (3.19) $\sigma_{yz} = 0$, for $y = \pm d$. Thus we satisfy the boundary conditions for the two horizontal surfaces and have the elastic fields due to the periodic array of dislocations along the y-axis.

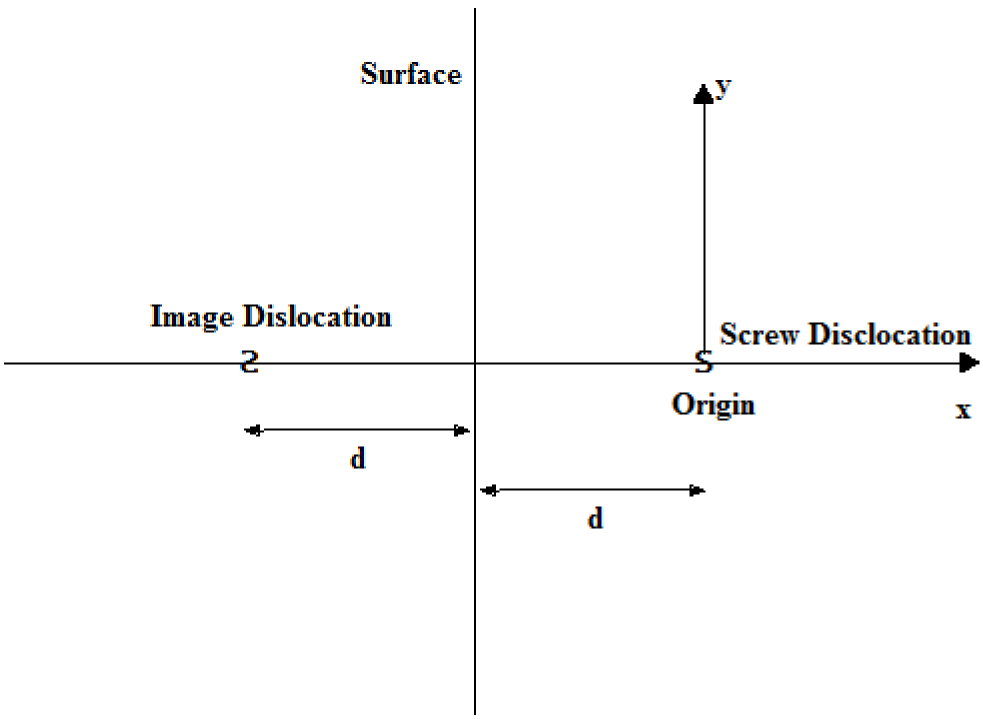

Figure 3.2: Screw dislocation along the z-direction located at the origin with the image dislocation located at a distance 2d and the surface at a distance d from the origin.

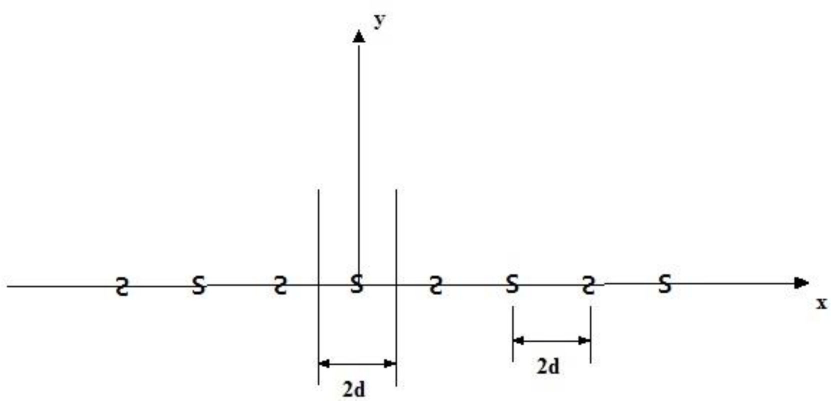

Figure 3.3: Periodic array of alternating positive and negative screw dislocations along the x-axis with 2d being the spacing between two dislocations of opposite nature and the crystal size (d is the distance from the free surface to the core of the dislocation. The core is at the origin).

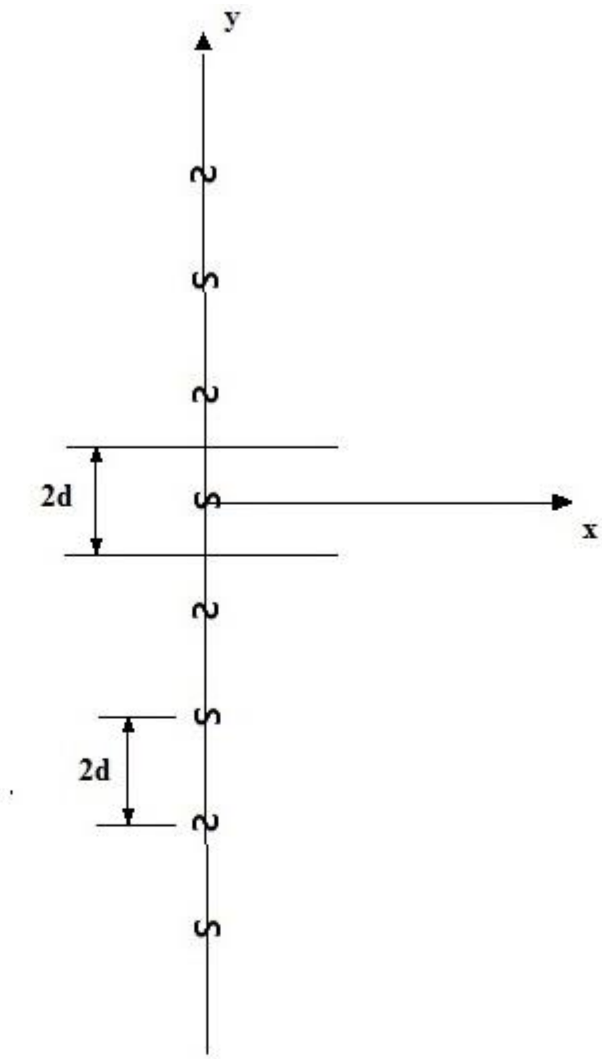

Figure 3.4: Periodic array of alternating positive and negative screw dislocations along the x-axis with 2d being the spacing between two dislocations of opposite nature and the crystal size (d is the distance from a free surface to the core of the dislocation. The core is at the origin).

Chapter 4: Intensity Contrast Simulations

4.1 INTRODUCTION

The problem of studying diffraction contrast from a screw dislocation in a transmission electron microscope can be resolved into two parts, (a) proposing a model for the displacement field u_z caused by the presence of the dislocation and (b) solving the Howie-Whelan Equations by numerical integration. The first part was addressed in Chapter 3, where we solved the displacement fields for three different cases, namely

1) No bounding surfaces: A single dislocation in an infinite crystal
2) One bounding surface: A single dislocation in a semi-infinite crystal
3) Two bounding surfaces: A periodic array of dislocations along the x-axis

For the second part of the problem we used Matlab to integrate the Howie Whelan equations discussed in Chapter 2. The code has been attached in Appendix A. To facilitate the integration in Matlab, the Howie Whelan equations can be written in dimensionless form, namely,

$$\frac{d\phi_0^{'}}{dY} = (-\frac{\xi_g}{\xi_o^{'}})\phi_0^{'} + (i - \frac{\xi_g}{\xi_g^{'}})\phi_g^{'} \tag{4.1}$$

$$\frac{d\phi_g^{'}}{dY} = (i - \frac{\xi_g}{\xi_g^{'}})\phi_0^{'} + (-\frac{\xi_g}{\xi_0^{'}} + 2is\xi_g + 2\pi i \frac{d(g.R)}{dY})\phi_g^{'} \tag{4.2}$$

The equations 4.1 and 4.2 may be integrated numerically starting with the initial conditions $\phi_o^{'}(0) = 1, \phi_g^{'}(0) = 0$ where (0) represents the top surface of the crystal. $\phi_0^{'}$ and $\phi_g^{'}$ are the amplitudes of the direct and diffracted beams, respectively. The variation of intensities $|\phi_o^{'}(\mathrm{t})|^2$ and $|\phi_g^{'}(\mathrm{t})|^2$ at the exit of the crystal and along the x-axis provides the diffraction contrast in the bright and dark field images, respectively (Figure 4.1).

4.2 INPUT PARAMETERS

The input parameters that go into the above equations have been explained in Chapter 2. These parameters depend upon the material and the diffracting conditions. The dimensionless term $\frac{\xi_g}{\xi_o'}$ is called the normal absorption coefficient. This coefficient takes into account the general reduction of the number of electrons in a column as a function of depth in the crystal. For a crystal of constant thickness, this parameter acts as a scaling factor for the intensities over the whole area of the image.

The dimensionless term $\frac{\xi_g}{\xi_g'}$ is called the anomalous absorption coefficient. This value depends on the diffracting vector g, as well as the crystal being examined. The amount of deviation from the Bragg condition may be represented by s or the dimensionless parameter $s\xi_g$. In this thesis, we have used 1) copper as a model system, 2) the diffracting vector g (111) and 3) an acceleration voltage of 200 kV. The parameters used in equations 4.1 and 4.2 are as follows [26].

$$\xi_g = \xi_{111} = 38.3nm$$

$$\xi_0' = 316.6nm$$

$$\xi_g' = \xi_{111}' = 316.6nm$$

$$\frac{\xi_g}{\xi_0'} = 0.121$$

$$\frac{\xi_g}{\xi_g'} = 0.0563$$

In order to validate the simulation program, the analytical and numerical solutions were first compared. Taking the input displacement fields to be zero, the analytical and numerical solutions were the same, thereby validating the code. The results are shown in figure 4.2.

4.3 PRACTICAL ASPECTS CONSIDERED IN THE SIMULATIONS

For an infinite crystal, the contrast width of a dislocation observed in a bright-field TEM micrograph is usually around 20nm. A TEM micrograph of a dislocation in an infinite crystal was taken and using imaging software a contrast profile was drawn across the width of the dislocation .This has been shown in Fig 4.3(a) and Fig 4.3(b). The width of the dislocation obtained from the TEM micrograph was seen to be around 15-20nm However, from a practical standpoint most of the samples used in microscopy have finite size. Thus, as discussed before, it is important to determine whether the contrast width of a dislocation is affected by crystal size. To address this issue, the intensity contrast simulations were carried out for the cases of an infinite crystal, a semi-infinite crystal and a finite crystal of various sizes.

In addition, when using diffraction contrast imaging in the TEM, the microscopic parameters play a very important role, in particular the deviation parameter w and the g.b diffraction conditions. Therefore, it is critical to analyze how the deviation parameter affects the contrast profiles for varying crystal sizes. In this thesis, I have investigated the cases of $w = -0.5, w = 0, w = 0.5$ for infinite, semi-infinite and finite crystals. In terms of g.b conditions, the cases of g.b=1 and g.b=2 are important. In the former, the best diffraction contrast is achieved, whereas in the latter the intensity contrast produces two dark lines (or two peaks), which may lead to a misinterpretation of the dislocation image. Hence, in this thesis, the effect of $g.b = 1$ and $g.b = 2$ g.b conditions were studied for the infinite, semi-infinite and finite cases for varying crystal sizes.

4.4 EFFECT OF CRYSTAL SIZE ON THE DIFFRACTION CONTRAST OF A SCREW DISLOCATION

4.4.1 The case of an infinite crystal

First, a single screw dislocation in an infinite crystal was considered and the intensity plots were analyzed. Figure 4.4 shows the intensity contrast simulations of a screw dislocation for $g.b = 1$ in the middle of a thick foil of thickness, $t = 8\xi_g = 306.4nm$ where *t* is the thickness of the foil. The middle of the foil is the simplest case to analyze when introducing the effect of crystal size. The thickness used was selected to simulate the case of an infinite crystal along the thickness.

Taking the case of the reflecting position ($w = s\xi_g = 0$), Figure 4.4 shows that the bright field and dark field intensity profiles are quite similar, where dislocations appear as dark lines against a white background. This could be explained by the fact that a fairly thick crystal was used and the effects of absorption are significant. The bright field profile is slightly asymmetrical along *x*, while the dark field intensity profile is symmetrical in *x* with its peak at the core of the dislocation.

In order to analyze and be able to achieve conclusive results from the diffraction contrast plots it is important to set a uniform intensity point to measure the width of the dislocation contrast profiles. In this regard the width was measured at 50%, 75% and at 90% of the maximum intensity.. This was compared with the width of the dislocation obtained from the TEM micrograph shown in Fig.4.2(a) which seems seemed to compare best to the value of the measured width at 90% of the maximum intensity for the dislocation contrast simulation. Based on this we have used the width at 90% for future analysis.

In addition as the intensity contrast dark field profiles for the infinite crystal are symmetric about the core of the dislocation, we have used these profiles in the subsequent sections. We will discuss next the case of a semi-infinite crystal.

4.4.2 The case of a semi –infinite crystal

A single screw dislocation in a semi-infinite crystal was now considered where a vertical surface was placed at varying distances from the core of the dislocation. Figure 4.5 shows a cumulative plot of intensity contrast simulations of a screw dislocation for varying semi finite widths. The screw dislocation was assumed to be in the middle of a thick foil of thickness $t = 8\xi_g = 306.4nm$, where *t* is the thickness of the foil. The diffraction conditions ($g.b = 1$) for this case were taken to be similar to that of the infinite crystal.

As shown in Figure 4.5, as the semi-infinite crystal size increases the width of the intensity profile becomes wider. When observing Figure 4.5, it can be seen that the predominant effect on the width of the dislocation contrast profiles happens on the side where the single vertical surface is introduced. This is more clearly shown in Figure 4.6, where the image width of the dislocation is plotted as a function of crystal size. Another observation that can be made from Fig 4.5 is that with reducing crystal size it is seen that the difference in intensity tends to reduce, thus resulting in poorer contrast.

This observation raises curiosity as to how the dislocation contrast profile would be affected if another surface was introduced on the other side of the dislocation, thereby simulating the effect of a finite crystal along the x-axis. This will be discussed next.

4.4.3 The case of a finite crystal

In the finite case, two vertical surfaces are placed on either side of the dislocation. This requires the use of a periodic array of dislocations to obtain traction free surfaces and thereby satisfy the boundary conditions. In Chapter 3 we calculated the displacement fields for the case of two vertical surfaces. The corresponding displacement field was input to the program and the simulations were run for varying crystal sizes.

The intensity plots were obtained from the solution of the Howie Whelan Equations (equations 4.1 and 4.2). The input displacement field for the case of two surfaces has been shown in equation 3.15.

The displacement field is a function of *d* (distance between dislocations in a periodic array or distance from the surface to the core), while the integration of the Howie Whelan Equations takes into account *t* (thickness of the crystal) and other microscopic parameters ($w = s\xi_g$, the deviation parameter, diffraction vector and the Burgers vector). As a result, the width of the dislocation contrast profile depends on these parameters. Keeping the microscopic parameters constant, the effects of *d* and *t* were studied. This was done by computing the widths (normalized values are shown in Table 1) for various *d* values ranging from 2.5 nm to 50 nm, while the thickness of the crystal was varied from 5nm to 500 nm.

For thicknesses greater than 250nm (in other words t>>d) we observe an asymptotic region where the image widths of the dislocation were only a function of *d* and as we increased *d* the width of the curves increased. This effect can be seen clearly in Fig 4.7

In the range where the sample thickness varies from 5 nm to 100 nm, the width at 90% intensity does increase with increasing *d*. However, it is clear that there is an impact of the crystal thickness on the intensity profile and thus we need to point out that our displacement field only takes into account two surfaces along the x axis to account for the traction free surfaces and does not consider traction free surfaces along the thickness. As a result, it can be concluded that in ranges where t (thickness) is far greater the d (distance from the surface to the core) there is a clear trend showing an increasing of dislocation width with increasing d.

The results shown in Figure 4.8 are a cumulative plot of dislocation contrast simulations for a periodic array of dislocation for varying finite widths. A thick foil of thickness $t = 8\xi_g \approx 300nm$ is used. As can be seen from Figure 4.8, as the crystal size increases the width of the intensity profile becomes wider. This is clearly shown in Figure 4.9, where it is evident that an increase in finite crystal size leads to an increase of the width of the dislocation contrast and eventually becomes constant as we approach the case of an infinite crystal. But when you look at Figure 4.8 it can be seen very clearly that with decreasing crystal size the differencing in intensity tends to reduce thus resulting in poorer contrast. Thus with reducing crystal size though we see a decrease in the width of the intensity profile , it is of a poorer contrast .

Now that we investigated how the width of the dislocation contrast profile is influenced by the finite crystal size, it is important to see how the microscopic parameters affect the contrast with changing crystal size. The effect of the deviation parameter and the g.b conditions will be discussed in the following sections.

4.5 Effect of the deviation parameter on the diffraction contrast of a screw dislocation

4.5.1 The case of an infinite crystal

Figure 4.10a represents the diffraction contrast profiles for the deviated condition $w = s\xi_g = 0.5$, while Figure 4.10b shows the case for *w=0* (reflecting position). Taking the case of the reflecting position in Figure 4.10b it can be seen that the bright field and dark field intensity profiles are almost similar and thus dislocations appear as dark lines. However, the intensity contrast shows a peak with a long tail (more noticeable for the deviated conditions in Fig.4.10a compared to Fig.4.10b) for the bright field case. Thus, it can be interpreted from the bright field profiles that the deviated condition with its sharper contrast (Fig 4.10a) is better for imaging in the case of an infinite crystal than the reflecting position. However in the case of dark field profiles the difference in intensity reduces for the deviated condition thus resulting in a poorer contrast than the case of the bright field profiles.

4.5.2 The case of a semi-infinite crystal

Comparing Figures 4.11(a)-(c) it can be seen that the diffraction contrast profiles for the deviated conditions become less sharp as the width of the semi-infinite crystal reduces compared to profiles at the reflecting position. One way of interpreting this is to take the case of a particular semi-infinite crystal width and obtaining a cumulative plot for the deviated conditions with respect to the reflected position (Fig. 4.12).

This means that for any value of w , as we reduce the semi-infinite crystal size, the dislocation contrast width is reduced but the imaging in the diffraction contrast mode would be best for the reflecting position compared to that of the deviated conditions, as the peaks for the reflecting conditions are sharper compared to their respective deviated positions. This observation is better supported for the case of two vertical surfaces, as will be discussed next.

4.5.3 The case of a finite crystal

Similar to the observation we made for the semi-infinite, for the finite case the dislocation contrast profiles for $w \neq 0$ (Fig 4.13) have a less distinct contrast compared to that of the reflected position shown in Figure 4.14. The contrast profiles for the deviated positions show sharper profiles as the width of the finite crystal size increases.

Using a similar approach of analysis as used in the case of the semi-infinite crystal a cumulative plot for the deviated conditions ,with respect to the reflected positions ,was obtained (Fig. 4.15). The results show that as we reduce the finite crystal size, the dislocation contrast width is reduced but the imaging in the diffraction contrast mode would be best for the reflecting position compared to that of the deviated conditions

4.6 Effect of G.B conditions on the diffraction contrast of a screw dislocation

For the case of an infinite crystal, intensity contrast profiles for $g.b = 1$ are characterized by a single peak, while for $g.b = 2$ there are two peaks as shown in Fig 4.16. Thus, it is important to analyze how the crystal size affects the intensity profiles for the condition of g.b=2.

We first look at the semi-infinite case. As shown in Fig 4.17 we can see that as the width reduces the intensity contrast profiles are affected but the two distinct peaks cannot be interpreted from the curves. Thus it would be ambiguous to draw a conclusion from the intensity profiles for the semi-infinite case.

In the case of the intensity contrast profiles for a crystal of finite size (Figure 4.18) we notice that for large crystal sizes we observed two distinct peaks. However as we reduce the crystal size to about 5 nm the contrast features shows a variation of less than 5% and thus the two peaks may not be visible by the naked eye when interpreting them.

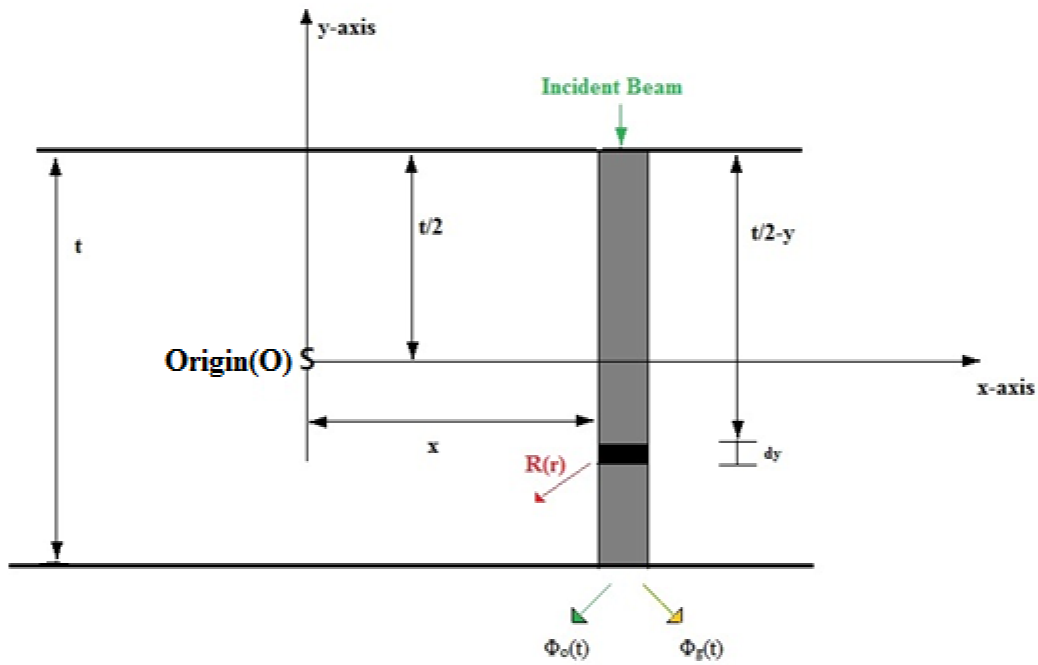

Figure 4.1: Coordinate system used to describe a screw dislocation in a crystal of thickness t. The effect of the strain field on the electron wave in the column at a distance x away from O (origin) is integrated in increments dy over its total thickness t, giving amplitudes ϕ_o and ϕ_g at the exit surface.

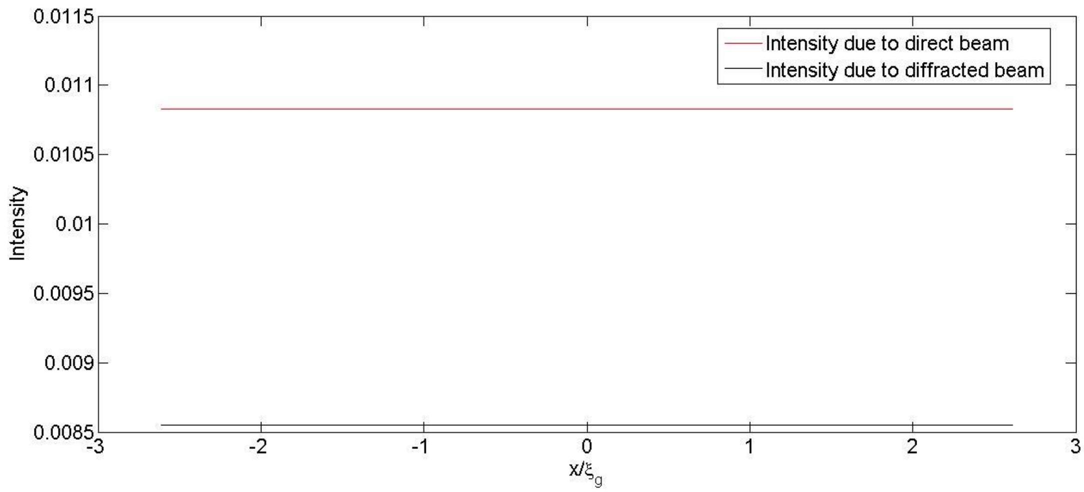

Figure 4.2: Analytical and real solutions provide the same intensity profiles (background intensity) when using a zero displacement field for g.b=1 and w=0 for the case of an infinite crystal of thickness $8\xi_g$.

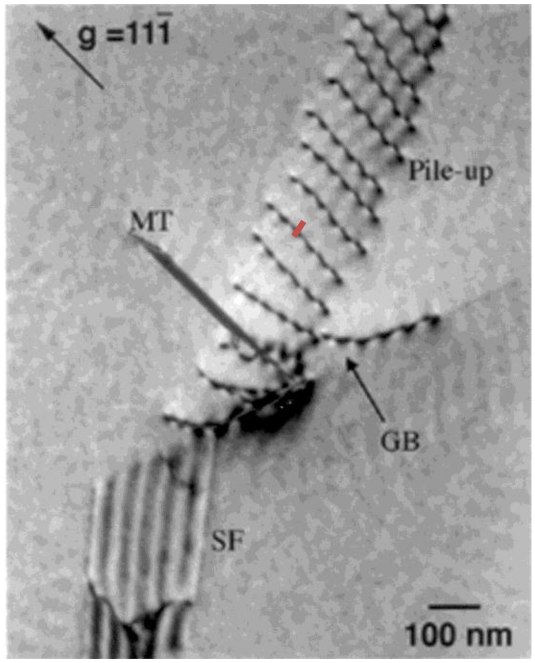

(a)

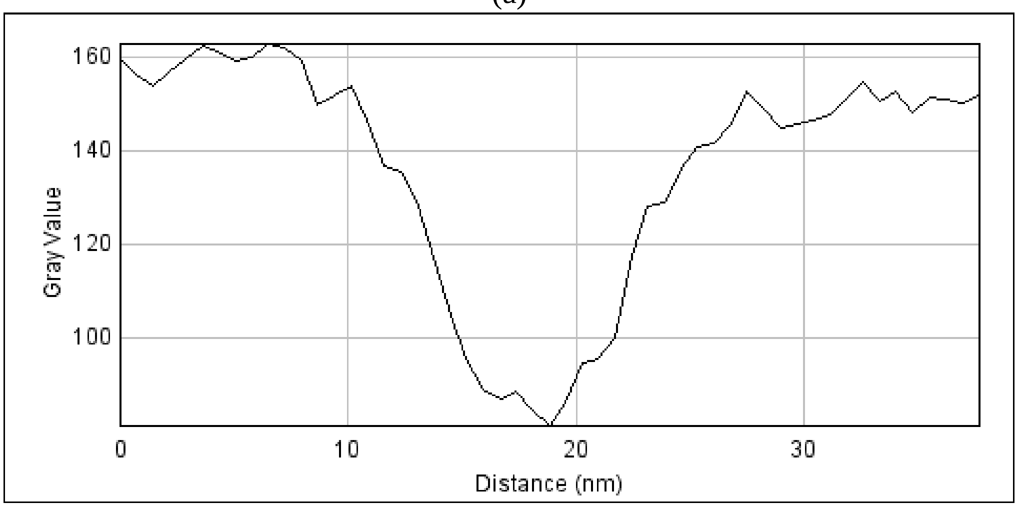

(b)

Figure 4.3: (a) TEM micrograph showing the presence of dislocation in a thick crystal [27] (b) Width contrast profile of the dislocation measured across the red line shown in a).

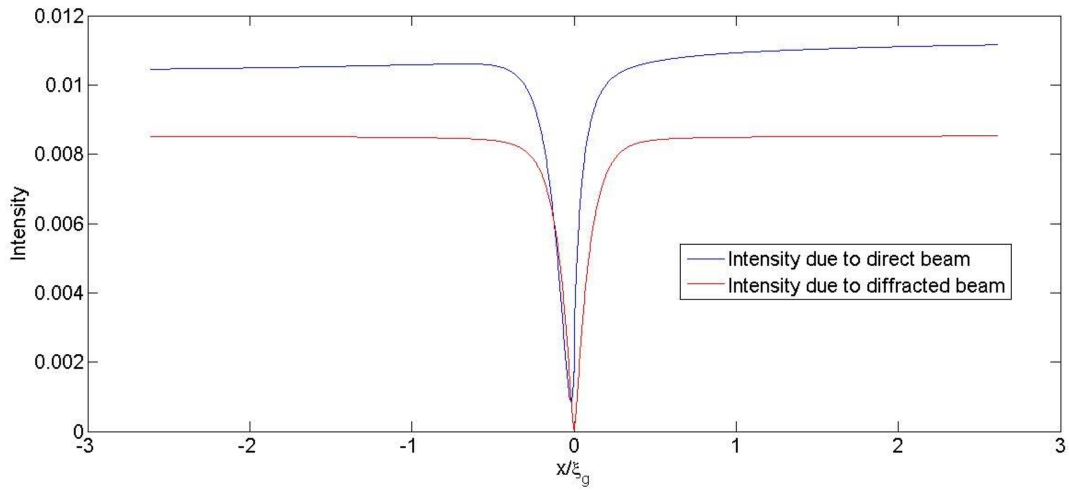

Figure 4.4: Computed bright-field (blue) and dark-field (red) intensity profiles for a screw dislocation in the middle of a thick foil with thickness of 306.4 nm. The parameters used are g.b=1 , w=0.

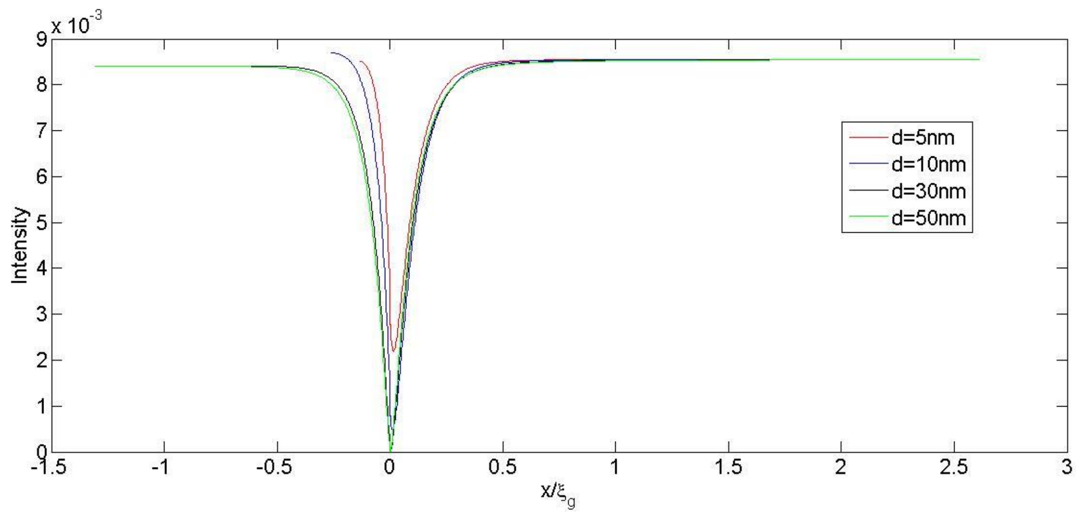

Figure 4.5: Computed dark-field intensity profiles for a single screw dislocation in a semi-infinite crystal with a vertical surface placed at varying distances from the core. The parameters used were g.b=0 and w=0.

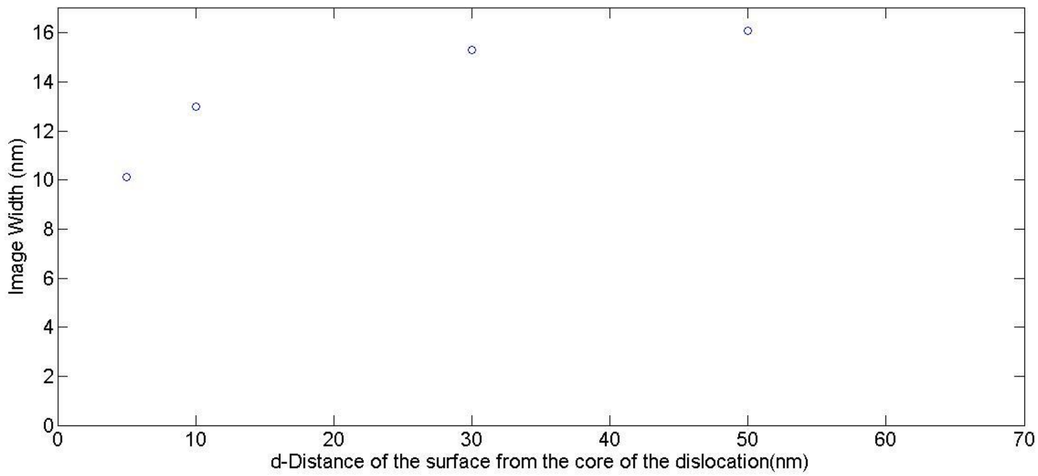

Figure 4.6: Image width of the dislocation vs the distance from the surfaces to the core of a screw dislocation in a semi-infinite crystal with the surface at varying distances from the core for the case of g.b=1.

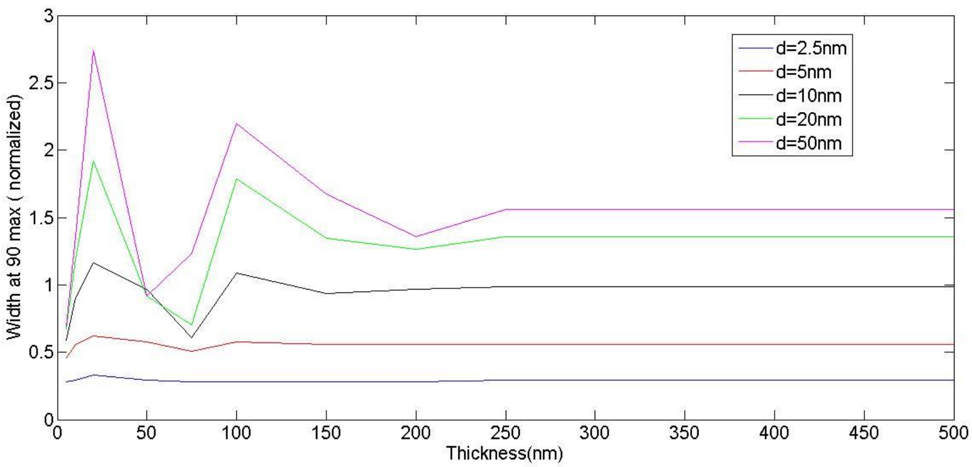

Figure 4.7: Image width at 90% of max. intensity vs thickness of different crystal sizes for the case of g.b=1.

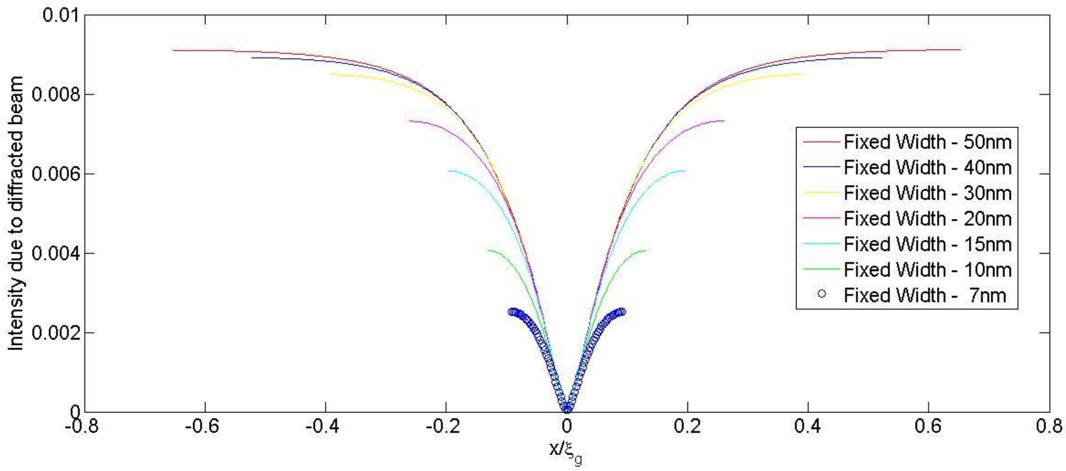

Figure 4.8: Computed dark-field intensity profiles for a periodic array of dislocations with the surfaces at varying distances from the core for the case of g.b=1 and w=0.

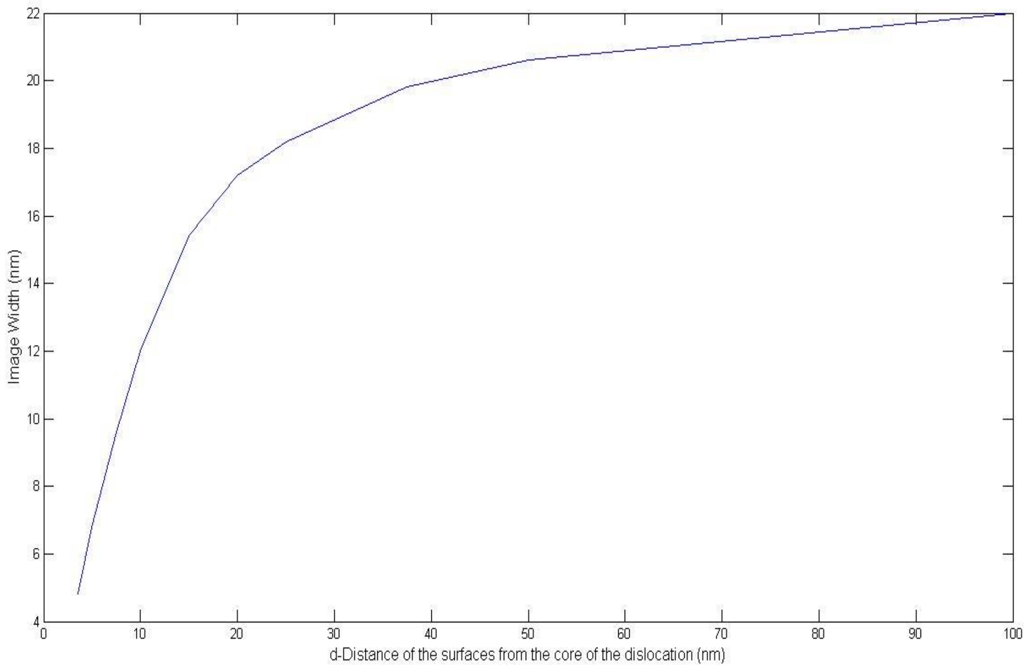

Figure 4.9: Image width of dislocation vs the distance from the surfaces to the core of the dislocation for the case of two vertical bonding surfaces with the surfaces at varying distances from the core for the case of g.b=1 conditions.

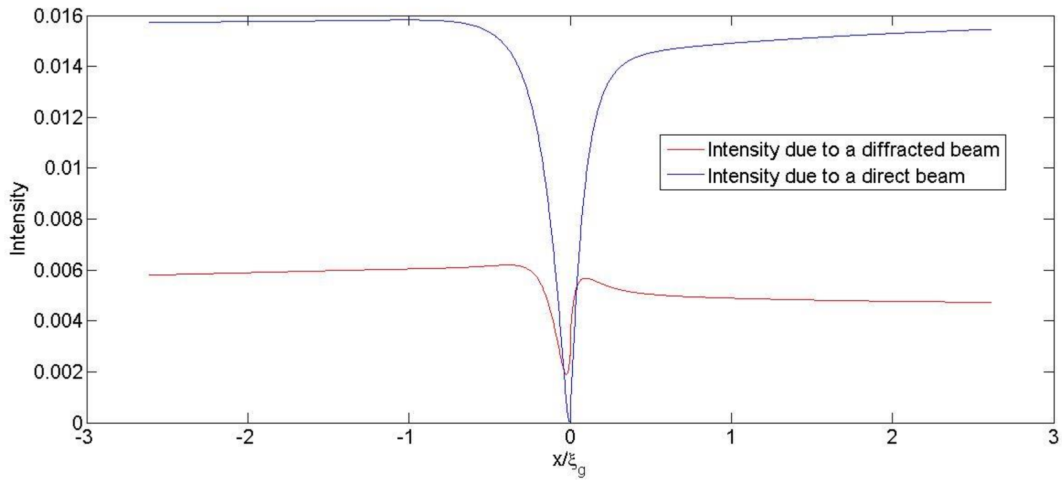

(a) w=0.5

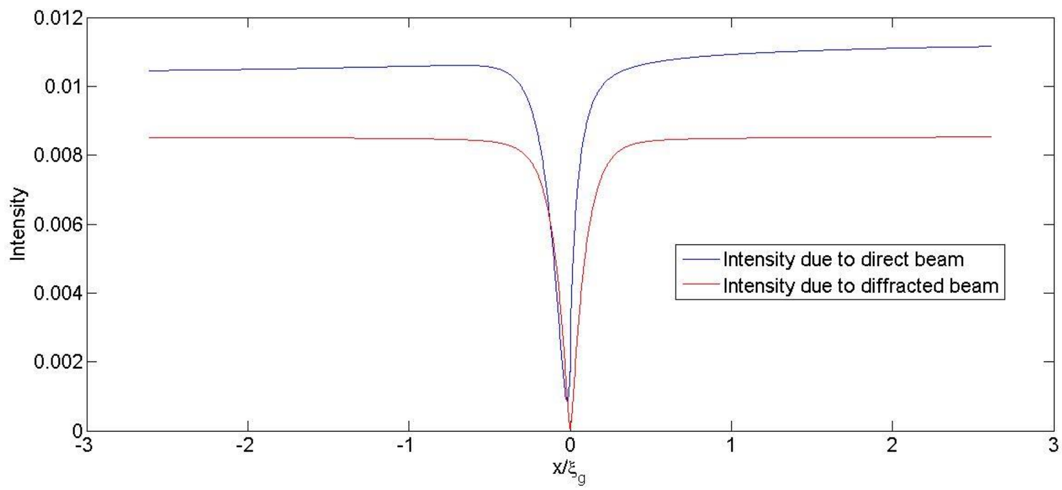

(b) w=0

Figure 4.10: Computed bright-field (blue) and dark-field (red) intensity profiles for a screw dislocation in the middle of a thick foil for g.b=1.

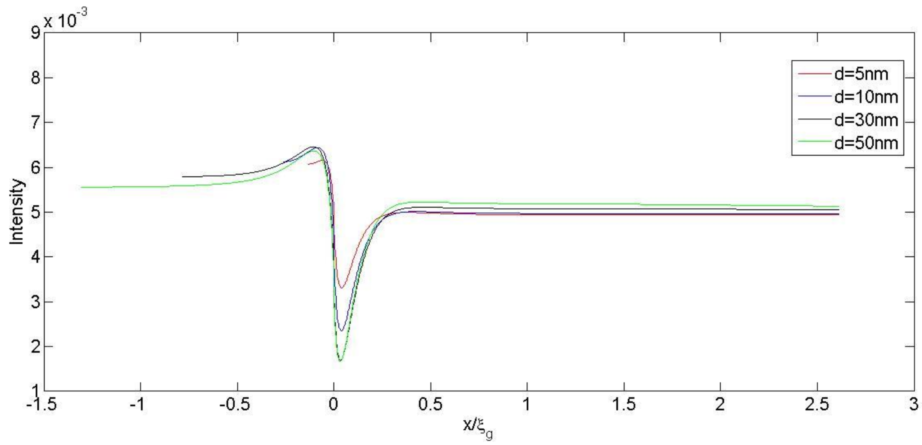

(a) w=-0.5

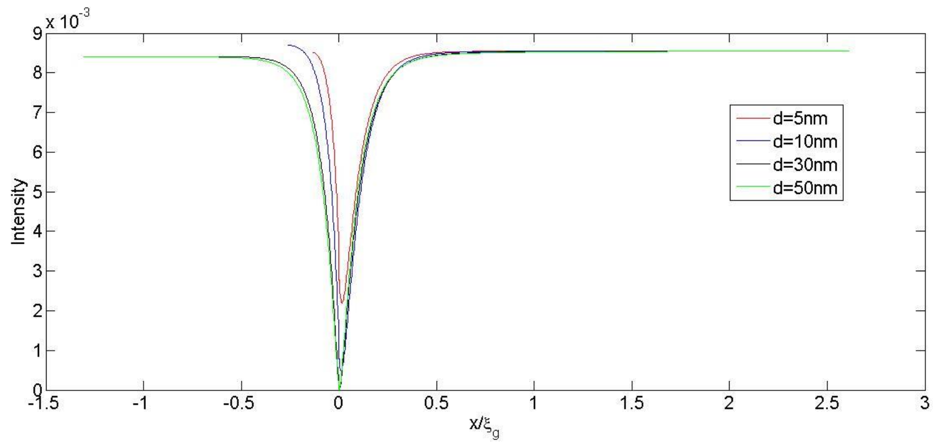

(b) w=0

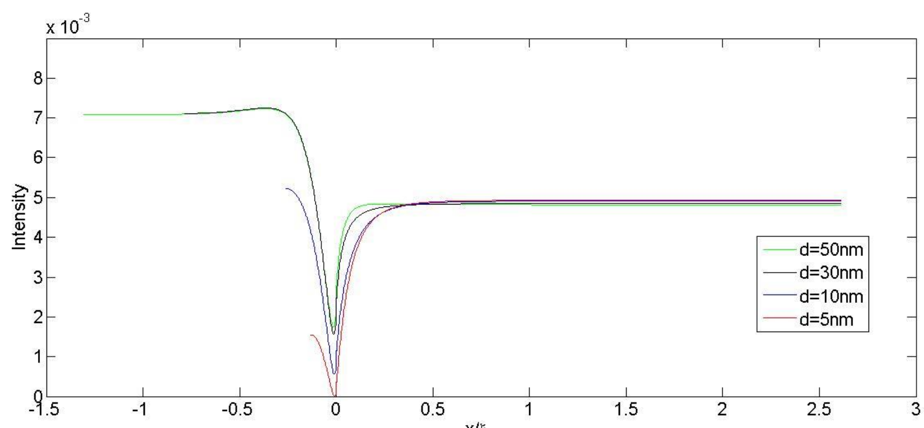

(c) w=0.5

Figure 4.11: Computed dark-field intensity profiles for a single screw dislocation in a semi-infinite crystal with the surface at varying distances from the core for the case of g.b=1.

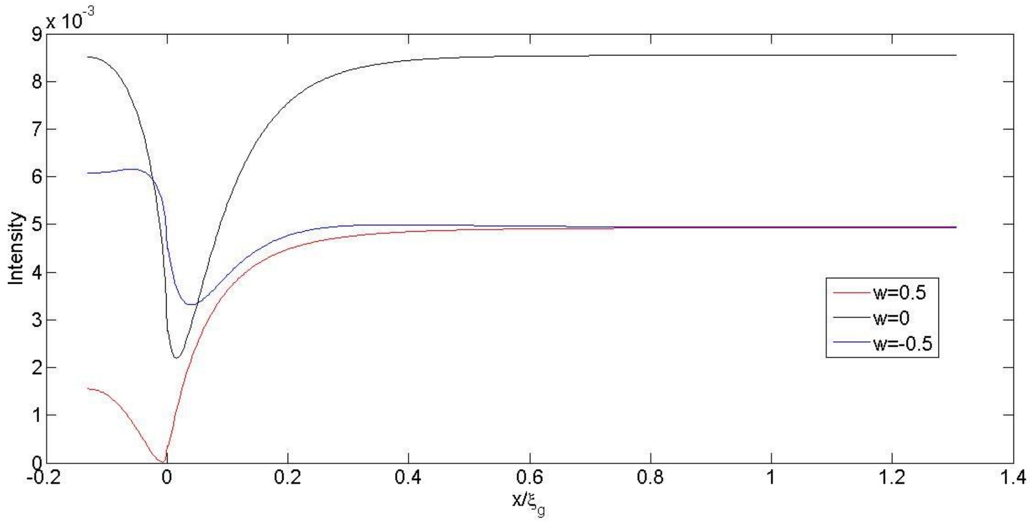

Figure 4.12: Cumulative dark-field intensity profiles for a single screw dislocation in a semi-infinite crystal with the surface at a distance of 5nm from the core, for the case of g.b=1.

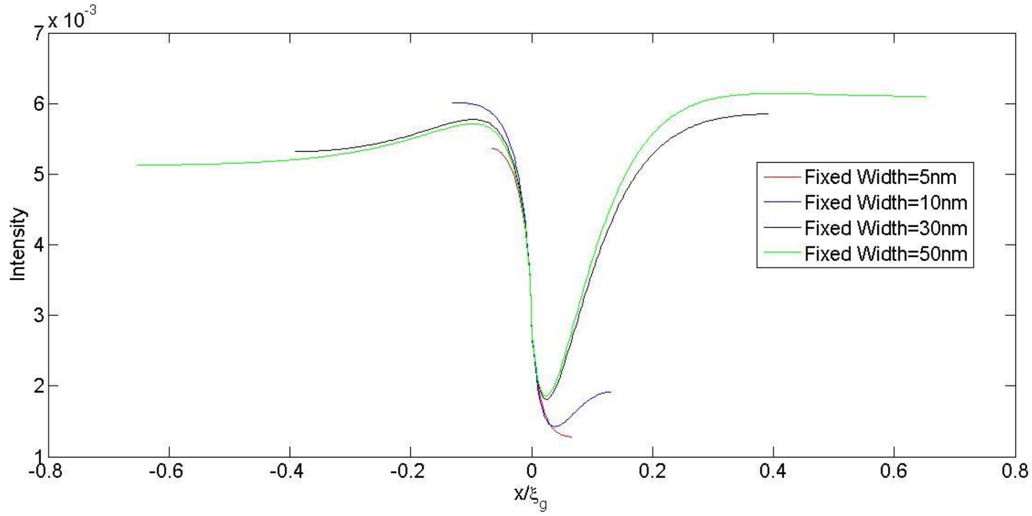

(a) w=-0.5

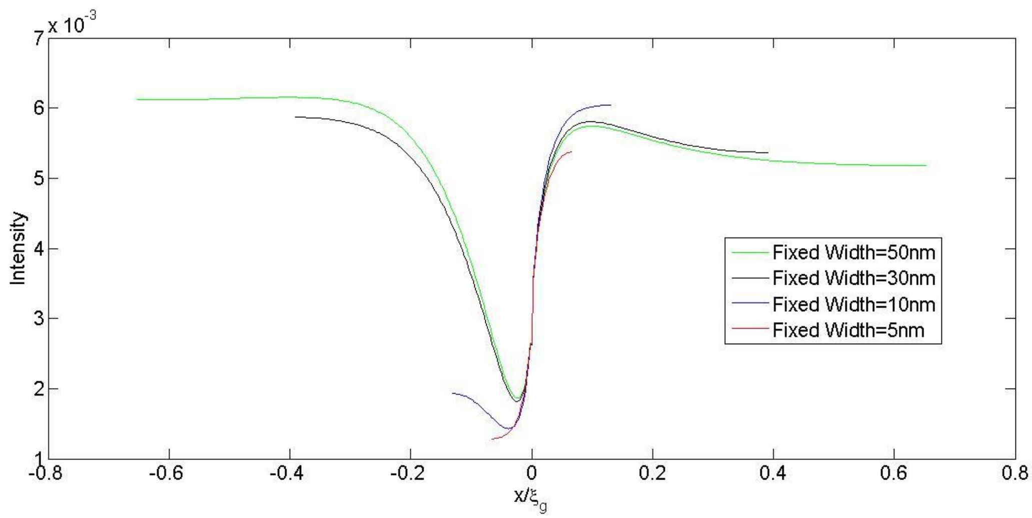

(b) w=0.5

Figure 4.13: Computed dark-field intensity profiles for two surfaces at varying distances from the core for the case of g.b=1.

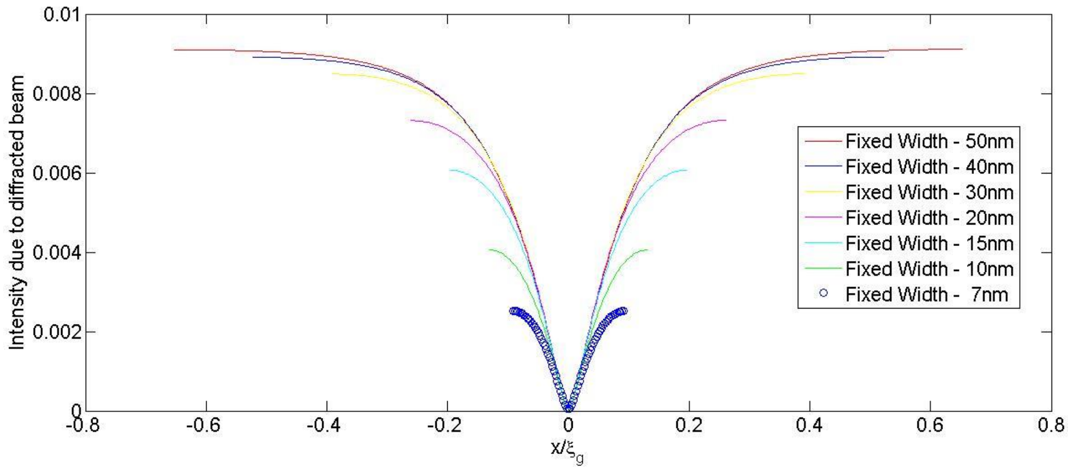

Figure 4.14: Computed dark-field intensity profiles for a periodic array of dislocations with the surfaces at varying distances from the core for the case of g.b=1 and w=0.

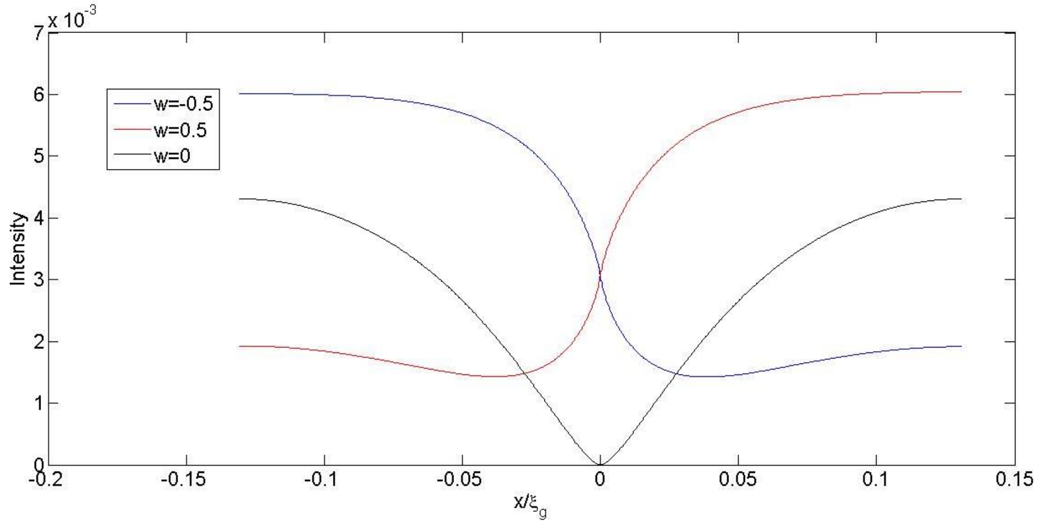

Figure 4.15: Cumulative dark-field intensity profiles for a single screw dislocation in a finite crystal with the surfaces at distances of 5nm from the core (crystal width is 10nm) for the case of g.b=1.

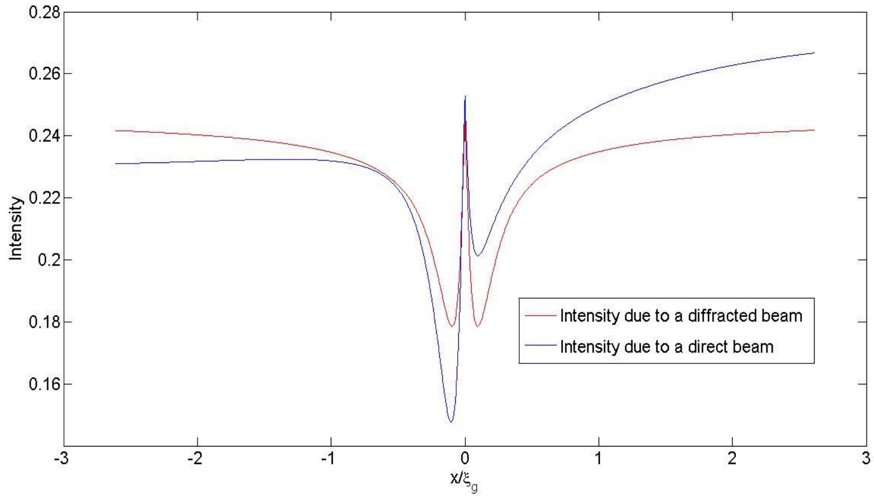

Figure 4.16: Computed bright-field (blue) and dark-field (red) intensity profiles for a screw dislocation in the middle of a thick foil for g.b=2 and w=0.

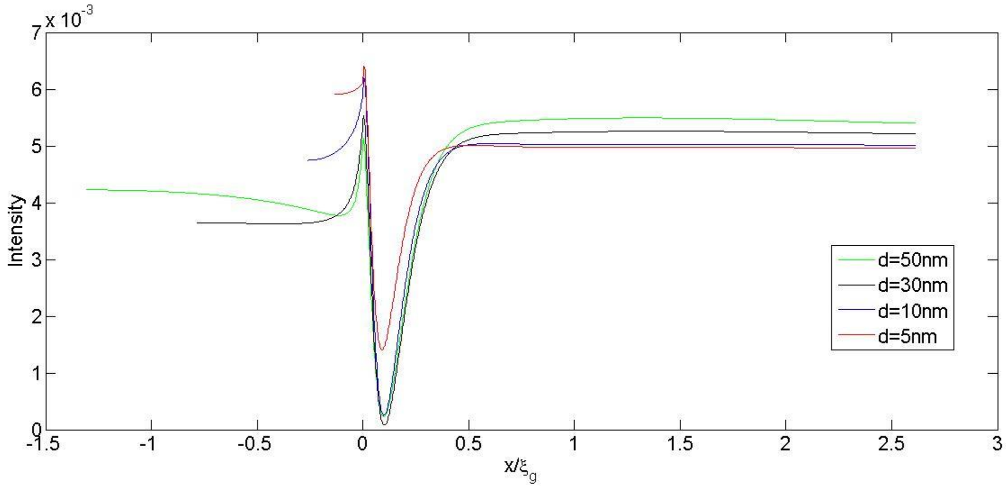

Figure 4.17: Computed dark-field intensity profiles for a single screw dislocation in a semi-infinite crystal with the surface at varying distances from the core for the case of g.b=2 and w=0.

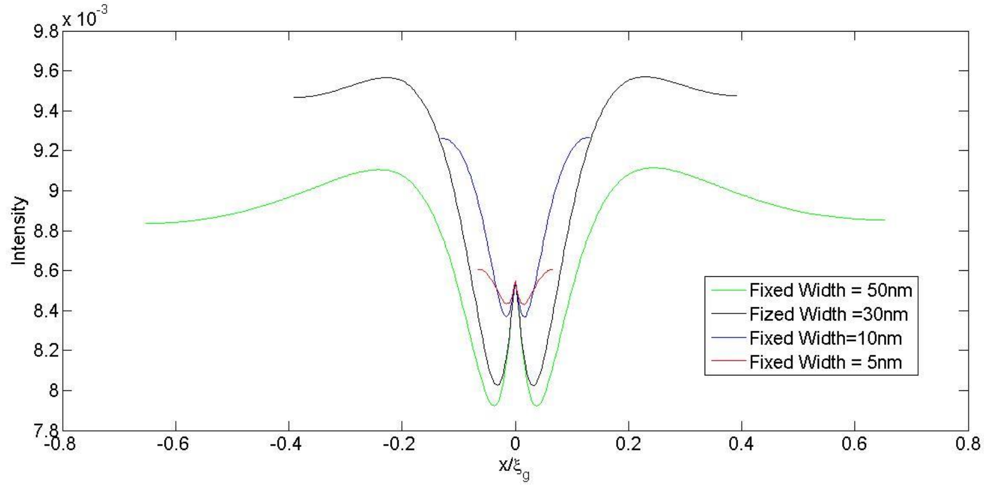

Figure 4.18: Computed dark-field intensity profiles for a periodic array of dislocations with the surfaces at varying distances from the core for the case of g.b=2 and w=0.

Chapter 5: Conclusions and Future Work

The objective of this work was to study the effect of crystal size on the diffraction contrast of a screw dislocation. The thesis shows that for the case of two vertical traction free surfaces surrounding the screw dislocation , as the size of crystal or the distance from the finite surfaces to the core of the dislocation was reduced, the image width of the dislocation was also observed. These conclusive trends were obtained for fairly thick crystals (>250nm). For thin crystals(<250nm) due to the absence of traction free horizontal surfaces , the trends observed as need to be further investigated.

The future direction of this work involves converting the intensity values obtained from the contrast simulations to computed simulated images. Using the existing Matlab code any elastic field calculations could be used as inputs.

Appendix A

The Matlab code used to obtain the intensity contrast simulation is shown:

The first m file is called the mfunctions

```
function [ yprime ] = myfunctions( z,y )
%myfunctions is the system of differential equations. z is a vector of z
%values and y is a vector of the initial conditinos of the system. Note: y(1)
%corresponds to the inital condition for T1 and y(2) corresponds to the inital
%condition for S1 and  y(3) is the value of x.

%Define Parameters of the System
N = 0.121;
A = 0.0563;
w = 0;

%Define B'. Note: y(5) is x and provided in the main function.
zd = 12.56;
 g = [1,1,1];
   b = 0.5*[1,1,0];
   d=5;

% The subroutine for the case of two bounding surfaces  B_prime = dot(g,b)* (
sin(pi*((y(3)/(2*d)))) /( cosh(pi*((z-zd)/(((d*pi)/38.3)*2))) - cos(pi*((y(3)/(2*d)))))- (
sin(pi*(((y(3)+2*d)/(2*d)))) /( cosh(pi*((z-zd)/(((d*pi)/38.3)*2))) -
cos(pi*(((y(3)+2*d)/(2*d)))))))/(8*((d*pi)/38.3));

% The subroutine for the case of one bounding surface B_prime= dot(g,b)* ( ((pi*y(3))/38.3) / (
(zd-z)^2+(((y(3)*pi)/38.3)^2)) -((pi*( 2*d +y(3)))/38.3) / ( (zd-z)^2+(((( 2*d +y(3))*pi)/38.3)^2)
))/(2*pi);

% The subroutine for the case of an infinite crystal B_prime= dot(g,b)*  ( ((pi*y(3))/38.3) / ( (zd-
z)^2+(((y(3)*pi)/38.3)^2)  ))/(2*pi);


yprime = [ -N*y(1)+(1i-A)*y(2); (1i-A)*y(1)+(-N + 2*1i*w + 2*pi*1i*B_prime)*y(2)
            0 % This is a dummy equation added only to be able
              %to pass the parameter x into ode45
              ];
end
```

The second mfile is called test.m

```
clear all
%This scrip runs ode45 on our differential equations and creates a plot.
```

```
%Parameters
zspan = [0,25.12]; %This is the z interval we want to plot
T_Intensity = [];
S_Intensity = [];
x = [-100:0.1:100];

for j = [1:max(size(x))]

y0 = [1,0,x(j)]; %These are the initial conditions of the system
         %Note: because of the way the system is defined in
         %myfunctions.m,y(1) is T1, y(2) is S1, and y(3) is x.
% options = odeset('MaxStep',1e-4);
[z,y] = ode45('myfunctions',zspan, y0);



T = y(:,1);
T2 = T.*conj(T);
S = y(:,2);
S2 = S.*conj(S);
T_Intensity(j,:) = T2(end)
S_Intensity(j,:) = S2(end)


end


 % plot((x),T_Intensity)
 % hold on
 % plot((x),S_Intensity,'r')
```

References

[1] Gerberich, W. W., et al. "Superhard silicon nanospheres." *Journal of the Mechanics and Physics of Solids* 51.6 (2003): 979-992.

[2] Volterra V. L'Equilibre des Corps Elastiques. *Annales scientifiques de l'Ecole normale superieure, Series 3* 1907; 24:401–517.

[3] Taylor GI. The Mechanism of Plastic Deformation of Crystals. *Proceedings of the Royal Society of London, Series A* 1934;145:362–405.

[4] Orowan E. Zur Kristallplastizitat. *Zeitschrift fur Physik* 1934; 89:605–659.

[5] Polanyi M. Uber eine Art Gitterstorungm die einen Kristall plastisch machen konnte. *Zeitschrift fur Physik* 1934; 89:660–664.

[6] Peierls RE. The size of a dislocation. *Proceedings of the Physical Society* 1940; 52:34–37.

[7] Cottrell AH. *Dislocations and Plastic Flow in Crystals*. Oxford Univ. Press: Oxford, 1953.

[8] Read WT. *Dislocations in Crystals*. McGraw-Hill: New York, 1953.

[9] Hirth JP, Lothe J. *Theory of Dislocations*. McGraw-Hill: New York, 1967.

[10] Nabarro FRN. *Dislocation in Solids*. North-Holland: Amsterdam, 1979.

[11] Mura T. *Micromechanics of Defects in Solids*. Martinus Nijhoff Publishers: Netherlands, 1982.

[12] Head AK. Edge Dislocations in Inhomogeneous Media. *Proceedings of the Physical Society, Section B* 1953; 66:793–801.

[13] Dundurs J, Mura T. Interaction between an edge dislocation and a circular inclusion. *Journal of Mechanics and Physics of Solids*1964; 12:177–189.

[14] Dundurs J. Elastic interaction of dislocation with inhomogeneities. In *Mathematical Theory of Dislocations*, ASME United Engineering Center: New York, 1969; 70–115.

[15] A.K Head, *Proc. Phys. Soc. B* 66 (1953) :793

[16] A.K. Head, Phil. Mag. 44 (1953) p.92.

[17] Khanikar, Prasenjit, Arun Kumar, and Anandh Subramaniam. "Image forces on edge dislocations: a revisit of the fundamental concept with special regard to nanocrystals." *Philosophical Magazine* 91.5 (2011): 730-750.

[18] Khanikar, Prasenjit, and Anandh Subramaniam. "Critical Size for Edge Dislocation Free Free-Standing Nanocrystals by Finite Element Method."*Journal of Nano Research* 10 (2010): 93-103.

[19] Sasaki, K., Kishida, M. and Ekida, Y. (2002), Stress analysis in continuous media with an edge dislocation by finite element dislocation model. Int. J. Numer. Meth. Engng., 54: 671–683.

[20] Williams, David B., and C. Barry Carter. *The Transmission Electron Microscope*. Springer Us, 1996.

[21] Hirsch, Peter Bernhard, et al. *Electron microscopy of thin crystals*. Vol. 320. London: Butterworths, 1965.

[22] Reimer, Ludwig, and Helmut Kohl. *Transmission electron microscopy: physics of image formation*. Vol. 36. Springer, 2008.

[23] Head, A. K. *Computed electron micrographs and defect identification*. North Holland, 1973.

[24] Hull, Derek, and David J. Bacon. *Introduction to dislocations*. Butterworth-Heinemann, 2001.

[25] Hirth, John P., and Jens Lothe. "Theory of dislocations." (1982).

[26] De Graef, Marc. *Introduction to conventional transmission electron microscopy*. Cambridge University Press, 2003.

[27] Paulo J.Ferreira, "Hydrogen Effects on crystal dislocations and stacking fault energy" , PhD Thesis UIUC, 1996